Article ID: 1000-324X(2017)07-0777-08 **DOI:** 10.15541/jim20160532

Effect of Gas-foaming Porogen-$NaHCO_3$ and Citric Acid on the Properties of Injectable Macroporous Borate Bioactive Glass Cement

WU Ying-Ying[1], YE Song[1], YAO Ai-Hua[1], LI Hai-Bin[1], JIA Wei-Tao[2], HUANG Wen-Hai[1], WANG De-Ping[1]

(1. School of Materials Science and Engineering, Tongji University, Shanghai 201804, China; 2. Department of Orthopaedic Surgery, Shanghai Sixth People's Hospital, Jiaotong University, Shanghai 200233, China)

Abstract: Borate bioactive glass (BBG) is a promising candidate material for bone tissue engineering. Mostly, it was applied in the form of scaffolds and granules. Till now, little work has been done to investigate the fabrication of porous borate bioactive glass cement (BBGC). In this work, we prepared an injectable macroporous BBGC *via* gas-foaming method, where $NaHCO_3$ and citric acid were used as porogen. Porous structure was analyzed by using SEM. The properties of soaking products were characterized by XRD, FTIR and ATR. The injection test showed that the injection rate of BBGC was over 80%. SEM images presented that there were apparent pores in BBGC. The diameter of the macropores varied from 10 μm to 800 μm. Furthermore, the degradability of BBGC was greatly improved. After one month *in vitro* soaking, the weight loss of non-foamed BBGC was only 50wt%, while for the foamed samples, their weight loss reached 70wt%. Meanwhile, the XRD, FTIR and ATR results exhibited that there were hydroxyapatite (HA) formation and confirmed that the introduction of macropores into the BBGC did facilitate the mineralization reaction.

Key words: gas-foaming; bioactive borate glass cement (BBGC); macropores; fast-degrading

Due to the advantages of excellent biocompatibility, degradability and osteoconductivity, borate bioactive glass (BBG) has attracted great interests in bone tissue engineering over the past decades. Specifically, BBG particles can react with body fluids and form a HA surface layer that bonds strongly to bone and soft tissue[1-2]. So far, BBG was mainly used in the form of scaffolds[3] and granules[4], but little work has been done to study the fabrication of borate bioactive glass cement (BBGC) .

Porosity and pore interconnectivity are of great importance in tissue engineering. It has been demonstrated that the introduction of pores into a bone substitute material facilitates its degradation and favors cell attachment, cell growth and cell differentiation[5-7]. As reported, porous borate glasses scaffolds promoted the proliferation of osteoblasts, supported the soft tissue ingrowth and was able to repair the skull defects after implanting into the rats subcutaneous[8]. Thus, the introduction of macropores into the BBGC is significant.

In addition, our research group had successfully prepared an injectable BBGC with excellent performance. However, the *vivo* implanting results indicated that the BBG's degradation behavior was poor, and only a small amount of newly bone formed on the surface of the implant[2, 9]. Based on the above rationale, we speculated that the introduction of macropores into BBGC can improve its degradation ability and accelerate mineralization rate. Furthermore, Chen, *et al*[10] and Thein-Han, *et al*[11] have successfully produced porous cement cylinders with interconnected pores *via* gas-foaming method, which had the advantages of easy-handing and easy-modulating[12].

The aim of this study was to develop an injectable porous BBGC *via* gas-foaming method, and to study the effect of porogen content on BBGC's handling properties and *vitro* soaking properties. Weight loss and pH changes during the conversion process were monitored, and the measurements of XRD, FTIR and ATR were carried out to characterize the conversion products.

1 Materials and methods

1.1 Preparation of BBGC

BBGC consisted of powder phase and liquid phase. Powder phase was a mixture of BBG powder and sodium bicar-

Received date: 2016-09-20; **Modified date:** 2017-01-04
Foundation item: National Natural Science Foundation of China (51372170, 81572105)
Biography: WU Ying-Ying (1992–), female, candidate of master degree. E-mail: tjclwyy2014@163.com
Corresponding author: WANG De-Ping, professor. E-mail: wdpshk@tongji.edu.cn

bonate ($NaHCO_3$), while liquid phase contained two parts: gelatin solution and corresponding citric acid. BBG with composition of $Na_2O{\cdot}8K_2O{\cdot}8MgO{\cdot}22CaO{\cdot}54B_2O_3{\cdot}2P_2O_5$; mol% was prepared by conventional melting and casting described before[9]. The mean size of BBG particle was 4.55 um. Gelatin (analytical grade; Sinopharm Chemical Reagent Co. Ltd., China) was dispersed at 6% (*w*/*v*) in 2.5wt% Na_2HPO_4 solution. Here, gelatin was used as a cohesion promoter. $NaHCO_3$ was added to BBG powder at $NaHCO_3$/BBG mass fractions of 0wt%, 5wt%, 8wt%, 10wt%, 12wt%, and 15wt%(see Table 1). The corresponding amount of $C_6H_8O_7{\cdot}H_2O$ was added to the deionized water to maintain a fixed $NaHCO_3$/($NaHCO_3$+$C_6H_8O_7{\cdot}H_2O$) mass fraction of 54.52wt%[13].

1.2 Handling properties of BBGC

The injectability of BBGC was tested *in vitro* using a method described previously[6]. BBGC pastes were prepared, and then transferred into a 5 mL syringe (diameter of needle=1.7 mm). The paste was pushed out at a crosshead speed of 15 mm/min using a mechanical testing machine (CTM 2500; Xieqiang Test Machine Inc., China) under the maximum applied force of 100 N. The percent of injectability (*I*) were calculated by the following equation:

$$I = \left[(M_o - M_1)/(M_o - M)\right] \times 100\% \quad (1)$$

Where M is the mass of the syringe, M_o is the mass of syringe filled with cement, and M_1 is the mass of syringe after extrusion.

The initial setting time of BBGC was determined according to ISO9917-1 by using a 400-G vicat apparatus with 1 mm diameter[14]. The setting time was calculated from the time when the powder phase mixed with the liquid phase to the time when the 400-g needle failed to create an indentation of 1 mm depth in three different areas. There were five specimens for testing in every sample.

The anti-washout properties means the ability of BBGC to harden in a dynamic aqueous environment without disintegrating into small pieces[15]. BBGC cylinders (6 mm in diameter×12 mm in height) were accurately weighted and directly tested in a gas bath thermostatic oscillator (CHA-SA; Xinbao Instrument Factory, China) shaking at 180 r/min. At selected times, cylinders were taken out for further observation. BBGC remaining integrally was collected, vacuum-dried and weighted. The disintegration resistance (*D*) was calculated by using the following equation:

$$D = \left(W_2/W_1\right) \times 100 \quad (2)$$

Where W_1 was the mass of the dried BBGC cylinder before soaking and W_2 was the weight of the integrally remaining BBGC cylinder at every selected time point.

Porosity measurements were performed on vacuum dried specimens. The percentage of porosity of each specimen was calculated according to the following calculating method.

$$\rho_{\text{apparent}} = \frac{m}{V} \times 100\% \quad (3)$$

Where m was the mass of dried specimen, V was its volume; ρ_{apparent} was the apparent density of BBGC specimen.

Assuming that there was no conversion reaction from BBG to the crystal, the true density of the specimen was calculated as following equation.

$$\rho_{\text{true}} = \frac{m_1 + m_2 + m_3}{m_1/\rho_1 + m_2/\rho_2 + m_3/\rho_3} \times 100\% \quad (4)$$

Where ρ_{true} was the true density of BBGC, m_1, m_2, m_3 represented the three different components containing in BBGC, and ρ_1, ρ_2, ρ_3 is the density of the corresponding components.

The total porosity, P_{total}, was obtained from the following equation:

$$P_{\text{total}} = \left(1 - \rho_{\text{apparent}}/\rho_{\text{true}}\right) \times 100\% \quad (5)$$

1.3 Soaking *in vitro*

BBGC cylinders (4.7 mm in diameter × 3.5 mm in height) were immersing in the PBS solution for soaking testing. The pH of the soaking solution was recorded at every selected time point using pH meter (pH-100 meter; Lichen Technology Inc., China). For the weight loss monitoring, specimens were removed from the PBS solution of every time interval, washed with demonized water three times and ethanol for the last time, vacuum-dried at 50℃ and weighed. Four specimens of each sample were measured each time.

After immersing in PBS, the soaking products could be determined by X-ray diffraction (XRD) (D/max-2500 VB2+/PC; Rigaku, Tokyo, Japan) and Fourier transform infrared spectroscopy (FTIR) and Attenuated Total Reflectance (ATR) (Bruker EQUINOX SS/ HYPERION 2000; Germany) in the wavenumber range of 400–2000 cm^{-1} and 600–4000 cm^{-1} on disks. The fracture surface morphology of BBGC was analyzed with a field emission scanning electron microscope (FESEM) (Hitachi S-4700; Tokyo, Japan). The specimens of BBGC were sputter-coated with gold prior to examination.

Table 1 Composition of the samples

Samples	S1	S2	S3	S4	S5	S6
BBG /g	1.5	1.5	1.5	1.5	1.5	1.5
($NaHCO_3$/ BBG) / %	0	5	8	10	12	15
Gelatin solution / mL	1.0	1.0	1.0	1.0	1.0	1.0
Citric acid / mL	0	0.2	0.2	0.2	0.2	0.2

2　Results and discussion

2.1　Handling properties of BBGC

The extrusion curves of BBGC showed that the injecting force rose with the increasing amount of porogen (see Fig. 1(a)). In addition, the injectabilities of all samples were excellent. Their injection rates were all above 80%, as shown in Fig. 1 (b). These phenomenona can be attributed to the repulsion between the particles, which greatly improved the particle flow ability[16-17].

Physical results of the BBGC were showing in the Table 2. The setting time decreased from (175 ± 15) min to (20 ± 2) min with the increasing amount of porogen, which was due to the usage of citric acid[18]. Citric acid was also called "water-reducing additive" of cement, which meant that there was more water available for the setting reaction. As compared with S1, the setting time of S2 was longer due to the introduction of macropores and higher Liquid/ Powder ratio. Besides, when the amount of porogen was 12%, the total porosity of BBGC reached 52%.

SEM micrographs of S2 and S4 were shown in Fig. 2. The macropores diameter of S2 was varied from 10 μm to 800 μm (see Fig. 2(a)) and for S4, they were in the range of 30-500 μm (see Fig. 2 (b)). The pores of both samples were interconnected. Except for the macropores connectivity, the connectivity between macropores and packing pores were in great proportion. What's more, Fig. 2(a) showed that S2 had larger pores size whereas the pore size distribution of S4 was more homogeneous. Besides, the BBG particles were wrapped by gelatin as can be seen from the Fig. 2(c) and 2(d).

The anti-washout ability of BBGC was considered to be an indicator of the degree of cement cohesion. The results showed the anti-washout ability of cements got improved with the porogen content increasing. However, the S2 exhibited the poorest anti-washout ability. Its weight loss reached 60wt% since it was disintegrated into small particles (see Fig. 3 and Fig. 4). Furthermore the excellent degradation ability of BBGC should be taken into account when calculating the disintegration resistance of BBGC.

2.2　*Vitro* soaking

Monitoring the weight loss of BBGC was one of the most effective ways to reflect its degradation behavior. Asshown in Fig. 5(a), all BBGC samples had alike degradation trend. Their weight loss rates were fast at first 10 d and then slowed down. Compared with S1 whose weight loss was only 50wt%, the weight loss of the foamed sam ples could reach 70wt% after one month immersion. As we can observe from Fig. 5(b), all samples showed similar variation trend at the first week, their pH

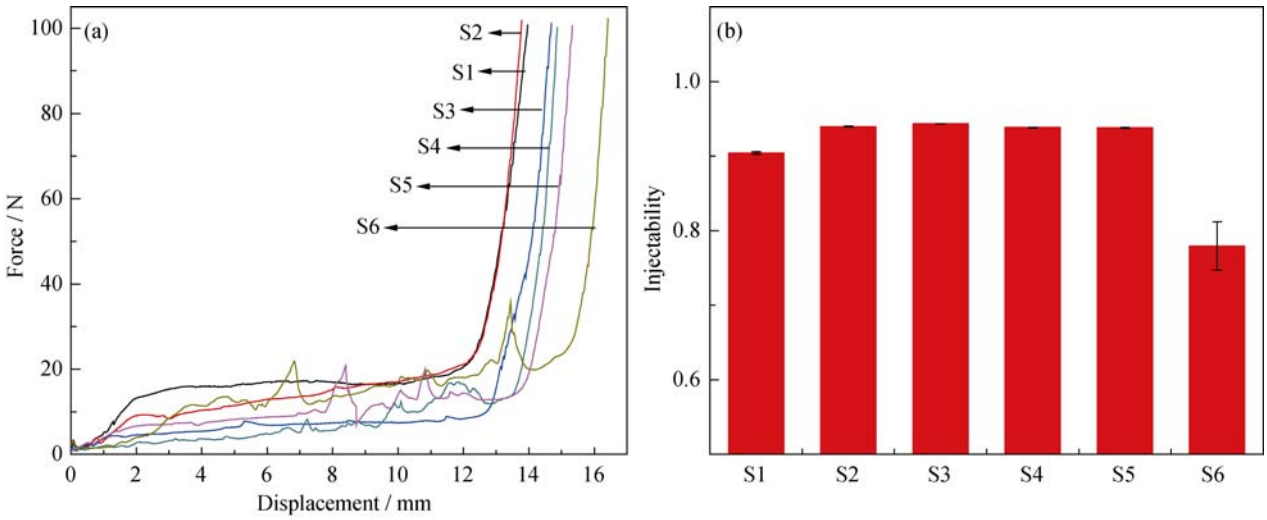

Fig. 1　Injectability study of the cements

(a) Representative injectability curves of BBGC with different porogen contents obtained from a syringe with a 1.7 mm diameter at a compression rate of 15 mm/min and maximum applied injection force of 100 N; (b) Injectability percentage measured for BBGC

Table 2 Physical results of the BBGC

No.	S1	S2	S3	S4	S5	S6
Setting time / min	110 ± 10	175 ± 15	82 ± 5	55 ± 5	25 ± 3	20 ± 2
Density / ($g \cdot cm^{-3}$)	1.10 ± 0.04	1.02 ± 0.02	1.04 ± 0.04	1.05 ± 0.04	0.98 ± 0.01	1.07 ± 0.04
Total porosity / %	47.07 ± 2.01	50.71 ± 0.85	49.38 ± 1.74	48.96 ± 2.13	52.18 ± 0.68	47.46 ± 1.89

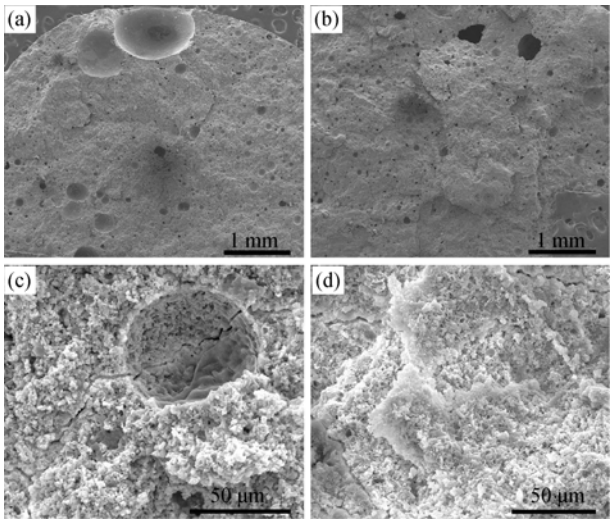

Fig. 2 Fracture surface morphologies of injectable BBGC after one day setting in water bath at 37℃
(a), (c) S2; (b), (d) S4

increasing from 7.4 to 9.0. Huang, *et al*[1] found that the pH variation of PBS was controlled by the process of solution precipitation reaction. Components in the BBG such as Na_2O and B_2O_3 dissolved into PBS to form Na^+ and BO_3^{3-} ions, whereas Ca^{2+} ions from BBGC reacted with PO_4^{3-} from PBS to precipitate, so the pH increased rapidly at the first week. After that, the precipitate products started consuming the OH^- ions and transforming into the HA, the pH decreased. The above results confirmed that BBGC was biodegradable, and the introduction of macropores did accelerate BBGC's degradability.

The final conversion products were analyzed by X-ray diffraction and FTIR technology. X-ray diffraction analysis of BBGC with varying soaking time showed strong differences in phase composition. Before immersion, the XRD pattern of S2 (see Fig. 6 (a)) showed no diffraction peaks. While after two weeks immersion, the major peaks in the pattern corresponded to those of standard HA (JCPDS 72-1243). The broad low-intensity peaks might be an indication that the as-formed HA had not fully crystallized or that the crystallite size of the HA product was in the nanometer range. Fig. 6(b) showed that the peaks increased in intensity after 30 d immersion, indicating that the conversion rate from reactants to apatite phase was accelerated with increasing porogen content of BBGC. It was worth mentioning that the diffraction peaks of S1 were still broad and relative weak in intensity even after 30 d-immersion. Fig. 6(d) showed the S1, S2, and S4 soaking products after 30 d's soaking. From

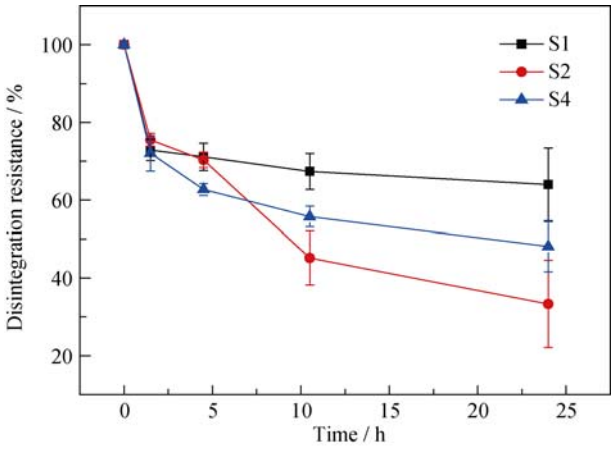

Fig. 3 Disintegration resistance of porogen-loaded BBGC after shaking for various times at 180 r/min in phosphate-buffered saline (PBS) at 37℃

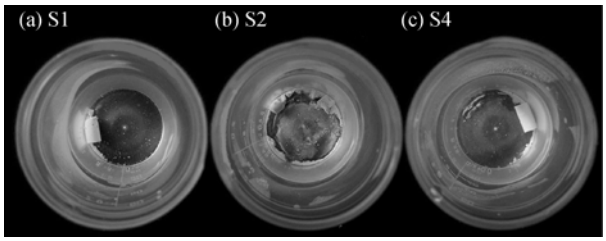

Fig. 4 Morphologies of injectable BBGC after soaking in PBS and shaking at 180 r/min for 24 h

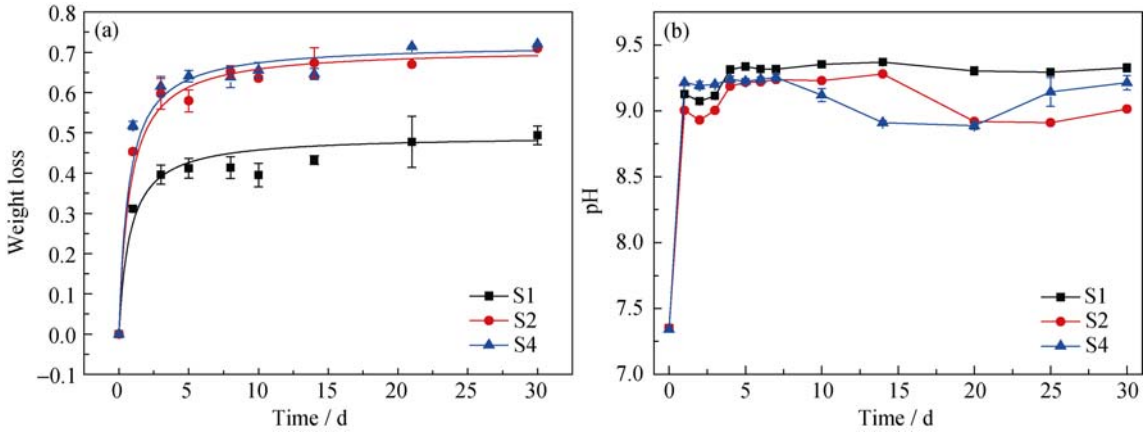

Fig. 5 Weight loss (a) and pH of PBS solution as a function of immersion time at 37℃ (b) of BBGC

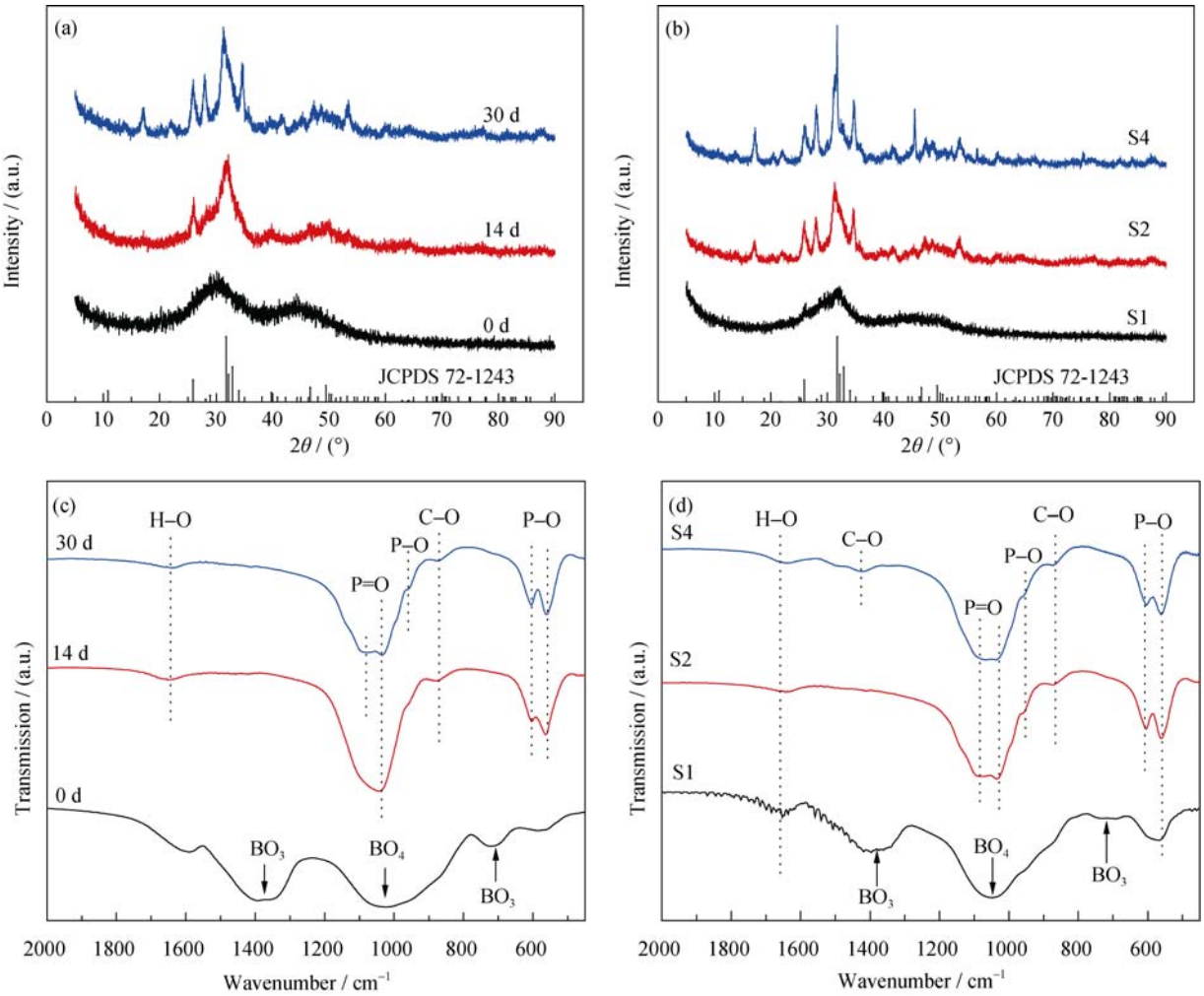

Fig. 6　XRD patterns of BBGC (a) and (c), S2 by immersing in PBS with different soaking time; (b) and (d) S1, S2, S4 after immersion in PBS for 30 d

the position and assignment of the peaks, the following characteristics could be pointed out. There were three broad resonances bands at 600–800, 800–1200 and 1200–1500 cm^{-1}, which can be assigned to the bending vibration of B–O–B in [BO_3] triangles, stretching vibration of the B_{IV}–O band in tetrahedral [BO_4] units and stretching of B_{III}–O in trigonal [BO_3] units[1, 9, 19], respectively. There were the characteristic resonances of BBG. In addition, the FTIR spectra also showed the major resonances characteristic of HA[20]. The resonances at 603 and 571 cm^{-1} corresponded to O–P–O symmetric stretching vibration in PO_4^{3-} groups in the HA lattice, and the resonances at 1045 cm^{-1} and 963 cm^{-1} were assigned to P–O stretching. While the band observed at 865 cm^{-1} was related to vibrational mode of CO_3^{2-} that was a characteristic of CO_3^{2-} substitution for PO_4^{3-}[21]. These results indicated that BBG gradually degraded and there was HA forming on the surface of BBGC. Furthermore, the characteristic bands of BBG can still be observed in FTIR spectra of S1 even after 30 d soaking, but for the foamed samples, the bands almost disappeared, indicating there were BBG powders residual in S1.

ATR proved to be more sensitive than the powder XRD technique, as the concentration of HA in the ATR sample was higher than that in the powder XRD sample. The ATR spectra of the inner and surface layer for the S1 and S4 as a function of soaking time were shown in Fig. 7. The spectra of the inner layer of S1 still exhibited strong characteristic resonances of BBG even after 21 d soaking, but for the surface layer, the intensity of those peaks decreased, and the P–O stretching peak at 1045 cm^{-1} gradually appeared with the increase of soaking time, as we can see from Fig. 7(a) and 7(b). As for the foaming sample S4, the resonance at 1045 cm^{-1} was observed for both inner layer and surface layer after 1 d soaking. Besides, the characteristic resonances of BBG almost disappeared, and the intensity of P–O stretching vibration increased after 21 d soaking, providing further indication for the formation of an HA layer on the surface of BBGC soaked in PBS. These results confirmed that the introduction of macropores into the BBGC greatly improved the degradability, and facilitated the mineralization reaction.

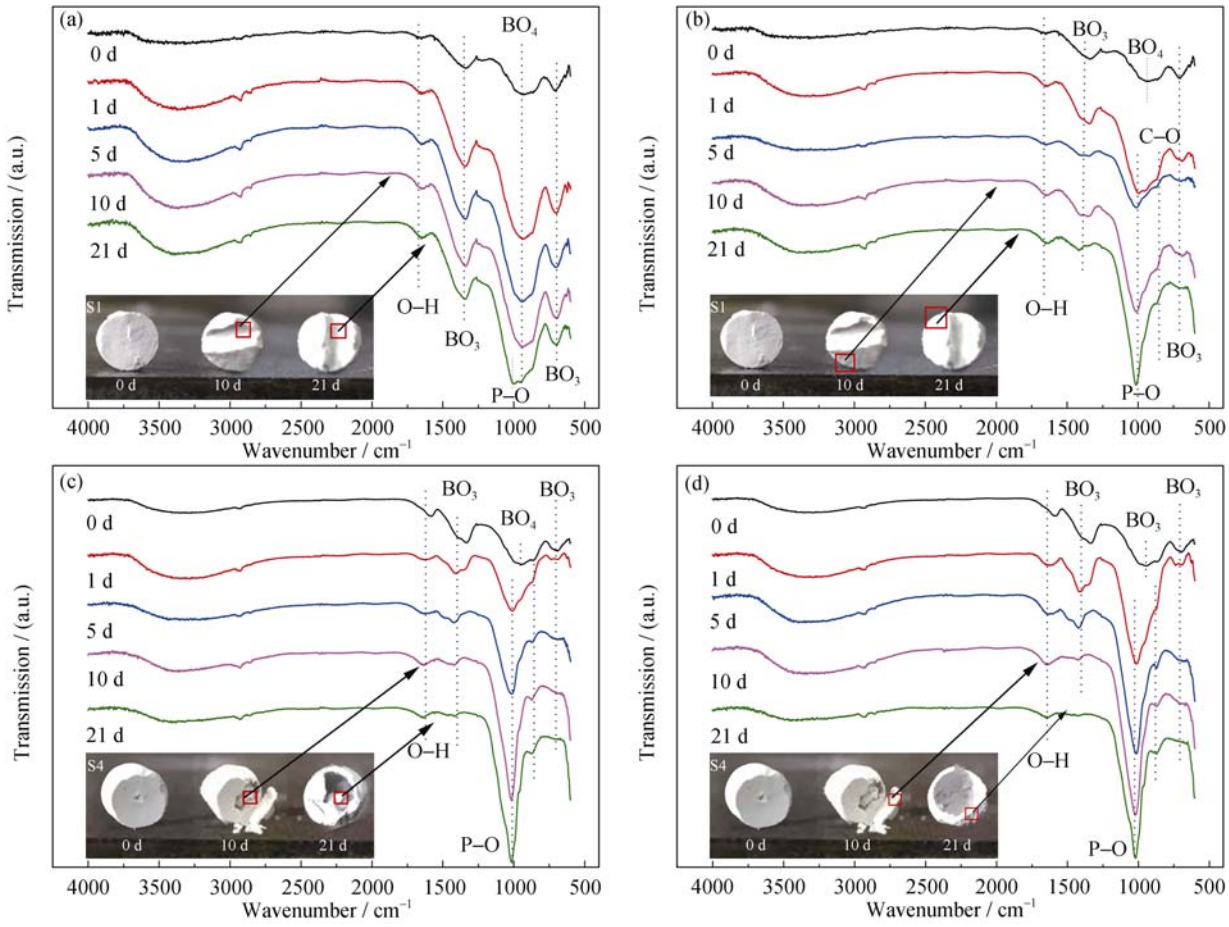

Fig. 7 ATR spectra of S1 and S4 as a function of soaking time (a), (c) materials 2 mm from the surface of S1 and S4 cylinder, respectively; (b) (d) surface materials of S1 cylinder and S4 cylinder, respectively

Fig. 8(a) showed that BBGC was a dense block before soaking. However, when soaking for a period of time, the BBGC cylinders' structure had changed. There was a hollow layer appearing between the surface layer and the inner layer of BBGC by observing the cross section of the soaking cylinders, as we can see from the photos in Fig. 7. This can be attributed to the lower chemical stability of BBG. When immersing in the PBS solution, the structure of BBG was broken, and then Na^+, Ca^{2+} and BO_4^{3-} ions would dissolve into the PBS solution. Therefore, the BBGC degraded. However, the dissolution of the glass, coupled with the the precipitation reaction. An amorphous calcium phosphate (ACP) layer formed and subsequently crystallized to Ha[22-23]. Apparently, the crystal structure of the precipitated composite was not so complete, so that the structure of the surface deposit was porous. Therefore, the PO_4^{3-} from the PBS solution could go through the porous payer and reacted with Ca^{2+} and formed a new layer of precipitated HA. There was no doubt that the thickness of the precipitated composite layer was increasing until the BBGC totally degraded as shown in Fig. 8(b). Furthermore, the content of Ca in BBGC was limited, at the same time, the PBS solution could not provide any other Ca^{2+}. Therefore, the structure of the final soaking products was hollow, as we can see from the Fig. 8(c).

3 Conclusions

In this research, we developed an injectable porous BBGC which had excellent handling properties and degradability. Based on our data, the introduction of macropores into BBGC greatly improved its degradability. The weight loss of foaming BBGC reached 70wt%, while the non-foaming one was only 50wt% in one month soaking. The XRD and FTIR results indicated that the conversion product was HA. The peaks of XRD increased in intensity with the porogen content increasing. What's more, the ATR results confirmed that the reaction mechanism between BBG and the PBS solution, which has been proposed by Huang, *et al*[1], and indicated that the introduction of macropores into the BBGC did accelerate the degradation process, and facilitate mineralization reaction. Furthermore, the setting time decreased greatly from (175±15) min to (20±2) min, whereas the injectability of cement was little minimized. Above all, the injectable po rous BBGC with 15% porogen developed in this study is a promising candidate.

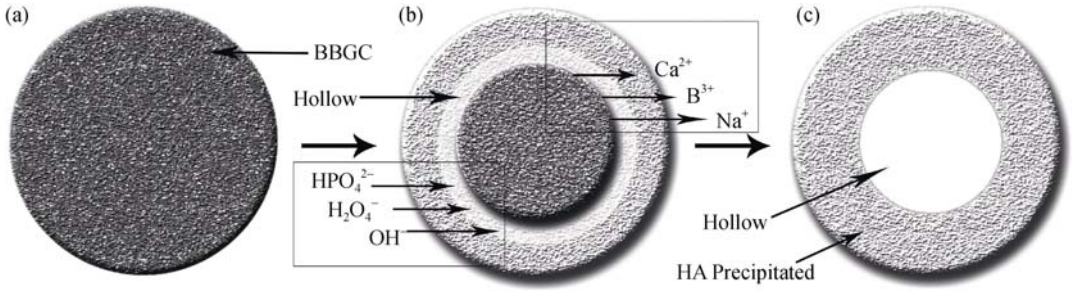

Fig. 8　Schematic illustration showing the degradation mechanism of BBGC in PBS solution as a function of times; sectional morphology of BBGC before soaking (a); BBGC soaking for some time (b); end product (c)

However, it was worth noting here that the degradability of the foaming BBGC was a little faster. In order to control the degradability of BBGC, future development should do more work on how to regulate the pore size distribution and porosity of the cement or consider to compound the CPC, which had low degradability, with the BBG.

References:

[1] HUANG W, DAY D E, KITTIRATANAPIBOON K, *et al*. Kinetics and mechanisms of the conversion of silicate (45S5), borate, and borosilicate glasses to hydroxyapatite in dilute phosphate solutions. *J. Mater. Sci-Mater. Med.*, 2006, **17(7):** 583–596.

[2] ZHANG Y, CUI X, ZHAO S, *et al*. Evaluation of injectable strontium-containing borate bioactive glass cement with enhanced osteogenic capacity in a critical-sized rabbit femoral condyle defect model. *ACS Appl. Mater. Inter.*, 2015, **7(4):** 2393–2403.

[3] LIANG W, RAHAMAN M N, DAY D E, *et al*. Bioactive borate glass scaffold for bone tissue engineering. *J. Non-Cryst. Solids*, 2008, **354(15):** 1690–1696.

[4] LOPES P P, GARCIA M P, FERNANDES M H, *et al*. Acrylic formulations containing bioactive and biodegradable fillers to be used as bone cements: properties and biocompatibility assessment. *Mater. Sci. Eng: C*, 2013, **33(3):** 1289–1299.

[5] INNOCENTINI M D M, FALEIROS R K, PISANI JR R, *et al*. Permeability of porous gel cast scaffolds for bone tissue engineering. *J. Porous Mat.*, 2010, **17(5):** 615–627.

[6] LANAO R P F, LEEUWENBURGH S C G, WOLKE J G C, *et al*. Bone response to fast-degrading, injectable calcium phosphate cements containing PLGA microparticles. *Biomaterials*, 2011, **32(34):** 8839–8847.

[7] KLIJN R J, VAN DEN BEUCKEN J J J P, FÉLIX LANAO R P, *et al*. Three different strategies to obtain porous calcium phosphate cements: comparison of performance in a rat skull bone augmentation model. *Tissue Part Eng. A*, 2012, **18(11/12):** 1171–1182.

[8] FU Q, RAHAMAN M N, FU H, *et al*. Silicate, borosilicate, and borate bioactive glass scaffolds with controllable degradation rate for bone tissue engineering applications. I. Preparation and in vitro degradation. *J. Biomed. Mater. Res. A*, 2010, **95(1):** 164–171.

[9] CUI X, ZHAO C, GU Y, *et al*. A novel injectable borate bioactive glass cement for local delivery of vancomycin to cure osteomyelitis and regenerate bone. *J. Mater. Sci-Mater. Med.*, 2014, **25(3):** 733–745.

[10] CHEN W, ZHOU H, TANG M, *et al*. Gas-foaming calcium phophate cement scaffold encapsulating human umbilical cord stem cells. *Tissue Eng. Part A*, 2011, **18(7/8):** 816–827.

[11] THEIN-HAN W W, XU H H K. Prevascularization of a gas-foaming macroporous calcium phosphate cement scaffold *via* co-culture of human umbilical vein endothelial cells and osteoblasts. *Tissue Eng. A*, 2013, **19(15/16):** 1675–1685.

[12] KIM H J, PARK I K, KIM J H, *et al*. Gas foaming fabrication of porous biphasic calcium phosphate for bone regeneration. *Tissue Eng. Regen. Med.*, 2012, **9(2):** 63–68.

[13] WU C, LUO Y, CUNIBERTI G, *et al*. Three-dimensional printing of hierarchical and tough mesoporous bioactive glass scaffolds with a controllable pore architecture, excellent mechanical strength and mineralization ability. *Acta Biomater.*, 2011, **7(6):** 2644–2650.

[14] CHEN C C, WANG C W, HSUEH N S, *et al*. Improvement of *in vitro* physicochemical properties and osteogenic activity of calcium sulfate cement for bone repair by dicalcium silicate. *J. Alloy Compd.*, 2014, **585:** 25–31.

[15] ZHANG J, LIU W, SCHNITZLER V, *et al*. Calcium phosphate cements for bone substitution: chemistry, handling and mechanical properties. *Acta Biomater.*, 2014, **10(3):** 1035–1049.

[16] YOKOYAMA A, YAMAMOTO S, KAWASAKI T, *et al*. Development of calcium phosphate cement using chitosan and citric acid for bone substitute materials. *Biomaterials*, 2002, **23(4):** 1091–1101.

[17] YAMAGUCHI I, IIZUKA S, OSAKA A, *et al*. The effect of citric acid addition on chitosan/hydroxyapatite composites. *Colloid. Surface. A*, 2003, **214(1):** 111–118.

[18] SARDA S, FERNANDEZ E, NILSSON M, *et al*. Kinetic study of

citric acid influence on calcium phosphate bone cements as water-reducing agent. *J. Biomed. Mater. Res.*, 2002, **61(4):** 653–659.

[19] DOWEIDAR H, EL-DAMRAWI G, AL-ZAIBANI M. Distribution of species in Na_2O–CaO–B_2O_3 glasses as probed by FTIR. *Vib. Spectrosc.*, 2013, **68:** 91–95.

[20] FATHI M H, HANIFI A, MORTAZAVI V. Preparation and bioactivity evaluation of bone-like hydroxyapatite nanopowder. *J. Mater. Process Tech.*, 2008, **202(1):** 536–542.

[21] PERUT F, MONTUFAR E B, CIAPETTI G, *et al*. Novel soy bean/gelatine-based bioactive and injectable hydroxyapatite foam: material properties and cell response. *Acta Biomater.*, 2011, **7(4):** 1780–1787.

[22] YAO A, WANG D, HUANG W, *et al*. *In vitro* bioactive characteristics of borate-based glasses with controllable degradation behavior. *J. Am. Ceram. Soc.*, 2007, **90(1):** 303–306.

[23] LIU X, RAHAMAN M N, DAY D E. Conversion of melt-derived microfibrous borate (13-93B3) and silicate (45S5) bioactive glass in a simulated body fluid. *J. Mater. Sci-Mater. Med.*, 2013, **24(3):** 583–595.

气体发泡剂—$NaHCO_3$和$C_6H_8O_7$对可注射多孔硼酸盐玻璃基骨水泥性能的影响

吴莹莹[1], 叶 松[1], 姚爱华[1], 李海滨[1], 贾伟涛[2], 黄文昆[1], 王德平[1]

(1. 同济大学 材料科学与工程学院, 上海 201804; 2. 上海交通大学附属第六人民医院 骨科, 上海 200233)

摘 要: 硼酸盐玻璃具有优异的生物相容性、降解性和骨传导性, 在骨组织修复领域受到一定的关注。目前, 硼酸盐玻璃的主要应用形式是支架和微球, 而有关硼酸盐玻璃基骨水泥的制备及性能研究却较少涉及。基于孔隙在骨组织修复材料工程领域中的重要作用, 本研究以 $NaHCO_3$ 和柠檬酸为气体发泡剂制备可注射的多孔硼酸盐玻璃基骨水泥, 通过 SEM、XRD 和 FTIR 等方法表征其对骨水泥性能的影响。结果表明: 发泡骨水泥具有良好的注射性, 其注射率高达 80%。SEM 形貌照片显示骨水泥中大孔已被成功引入, 且孔隙连通, 其孔径介于 10 μm 到 800 μm 之间。浸泡结果表明, 发泡骨水泥失重率明显提高。PBS 溶液中浸泡 30 d 后, 发泡骨水泥的失重率高达 70%, 而非发泡的骨水泥的失重率只有 50%。此外, XRD 和 FTIR 的结果表明, 浸泡产物为羟基磷灰石(HA)。ATR 的结果进一步证明了 BBG 和 PBS 溶液的反应机理, 表明 BBGC 中孔隙的引入大大加快了其降解, 促进了矿化反应的进行。

关 键 词: 硼酸盐玻璃基骨水泥; 气体发泡; 大孔; 快速降解

中图分类号: TQ171 **文献标识码:** A